WAKE EFFECTS ON POSITIVELY CHARGED SPACECRAFT IN FLOWING TENUOUS PLASMAS: CLUSTER OBSERVATIONS AND MODELING

Erik Engwall
Swedish Institute of Space Physics
Box 537, SE-751 21 Uppsala, Sweden
E-mail: **Anders.Eriksson@irfu.se**

Anders Eriksson
Swedish Institute of Space Physics

Arne Pedersen
Department of Physics, Oslo University, Norway

Julien Forest
Swedish Institute of Space Physics

Goetz Paschmann
Max-Planck-Institut für Extraterrestrische Physik, Germany

Jack Quinn
Roy Torbert
Space Science Center, University of New Hampshire, USA

Klaus Torkar
Space Research Institute, Austrian Academy of Sciences, Austria

Abstract

Comparison between electric field measurements made by the double-probe and electron drift instruments on the Cluster satellites have revealed significant perturbations in the signals from the electrostatic probes when Cluster is on magnetic field lines above the Earth's polar cap. In this region, there is a tenuous upflowing plasma known as the polar wind. The polar wind flow is supersonic, so a wake may form behind spacecraft structures. Usually, one expects wakes to be a problem mostly in denser plasmas. However, in this very tenuous environment, the spacecraft potential exceeds the kinetic energy of the ions (flow and thermal), so that the effective size of the wake is determined not by the spacecraft structures themselves, but by the potential distribution around them. As the plasma is tenuous, this is essentially the vacuum potential, which can extend very far from spacecraft structures. In particular, wire booms increase their effective size from the order of millimetres to the order of meters when the electrostatic effect is taken into account. We show the data to be qualitatively consistent with this interpretation. In particular, an observed alleviation of the effect when artificial potential control is applied lends strong support. Preliminary results of quantitative modeling and simulations provide additional insight.

Introduction

Spacecraft-plasma interaction studies usually focus on spacecraft charging to levels of kilovolts, as such potentials are an obvious source of technical problems for any spacecraft, particularly if different parts of the spacecraft charge to different voltages. In this study, we

will be concerned with much lower voltages, on the order of volts rather than kilovolts, occurring on conductive spacecraft where differential charging is not an issue. While this level of potential poses no danger to the physical health of a spacecraft, it can be a source of problems for scientific instruments intended for the study of plasmas in this energy range. Our particular concern in this paper will be a wake effect observed in cold tenuous plasmas by the electric field instruments on the Cluster spacecraft.

Each of the four Cluster spacecraft carries two instruments designed for measuring the electric field using different techniques, the double-probe Electric Fields and Waves instrument (EFW) (Gustafsson et al., 1997; Gustafsson et al., 2001) and the Electron Drift Instrument (EDI) (Paschmann et al., 1998; Paschmann et al., 2001). The performance of these two instruments have recently been compared by Eriksson et al. (2003). An interesting finding is that if a tenuous plasma (where the spacecraft potential V_s is positive due to photoemission) is so cool that the ions do not have sufficient energy to reach the spacecraft, the double-probe instrument EFW indicates apparent electric fields not seen by EDI. The observations were qualitatively understood in terms of a wake forming in the cold plasma, with a size determined not directly by the physical structure of the spacecraft but by the positive potential distribution around it.

In order to make this qualitative understanding a quantitative foundation, we need simulations of the plasma flow close to the spacecraft. The present paper is a report of initial results from such a simulation effort, using the open source particle-in-cell code package PicUp3D (Forest et al., 2001). This software is intended for workstations rather than supercomputers, and is excellently portable thanks to being written in Java. While this does not maximize the computational power, it simplifies the use of the code for engineers and scientists being able to run it on their own PCs. The primary aim of this study is to understand the EFW-EDI discrepancy, but a secondary goal is to verify that PicUp3D is useful for this kind of investigations. In Section 2, we show some Cluster data illustrating the problem, and introduce the qualitative model. The code and the simulations are presented in Section 3, with a concluding discussion in Section 4.

Enhanced Electrostatic Wakes in Cluster Data

Cluster is a mission designed for four-point measurements in key regions of the terrestrial magnetosphere and its adjacent environment in the solar wind (Escoubet et al., 2001), in particular boundary layers like the bow shock and the magnetopause. Thanks to its polar orbit with perigee at 4 RE and apogee at 19.6 RE, Cluster samples a broad range of plasma regions, from the cold and dense plasmasphere to the hot and tenuos plasma sheet. The four spacecraft were designed with identical payloads, each carrying a complete instrumentation for the study of particles and fields. For electric field measurements, Cluster includes two instruments using different techniques. The Electric Fields and Waves instrument (EFW) (Gustafsson et al., 2001) uses the well-known technique of measuring the voltage between spherical electrostatic probes at the ends of wire booms in the spacecraft spin plane (Pedersen et al., 1997). The technique allows sampling to essentially unlimited frequencies and can operate under widely varying plasma conditions, though great care is needed in the design in order to minimize disturbances from the spacecraft and the probe supports. EFW has two pairs of wire booms (2.2 mm diameter), with a distance of 88 m between opposite spherical probes (8 cm diameter). The Electron Drift Instrument (EDI) (Paschmann et al., 2001) uses a completely different technique (Paschmann et al., 1998), relying on observing the drift of electron beams emitted from the spacecraft and returned by the ambient magnetic field,

which thus has to be sufficiently strong for the method to work. Using electrons in the keV range, this technique is quite immune to any effects of spacecraft-plasma interactions in the eV range of energies. The Cluster spacecraft themselves are cylindrical, with radius 1.5 m and height 1.1 m.

The limitations of the two techniques for E-field measurements are quite different, and so they complement each other well. The EDI-EFW comparisons by Eriksson et al. (2003) showed the expected merits and weaknesses of each technique. To cite some examples, dynamic regions like the auroral zone are usually better covered by EFW because of its high sampling frequency and insensitivity to rapid variations of the background fields, while EDI often produces better data for small-amplitude electric fields in regions with cold plasma that perturb the EFW measurements. This happens particularly when the plasma is so cool that the ions cannot reach the spacecraft, which always is at a positive potential in the case of Cluster.
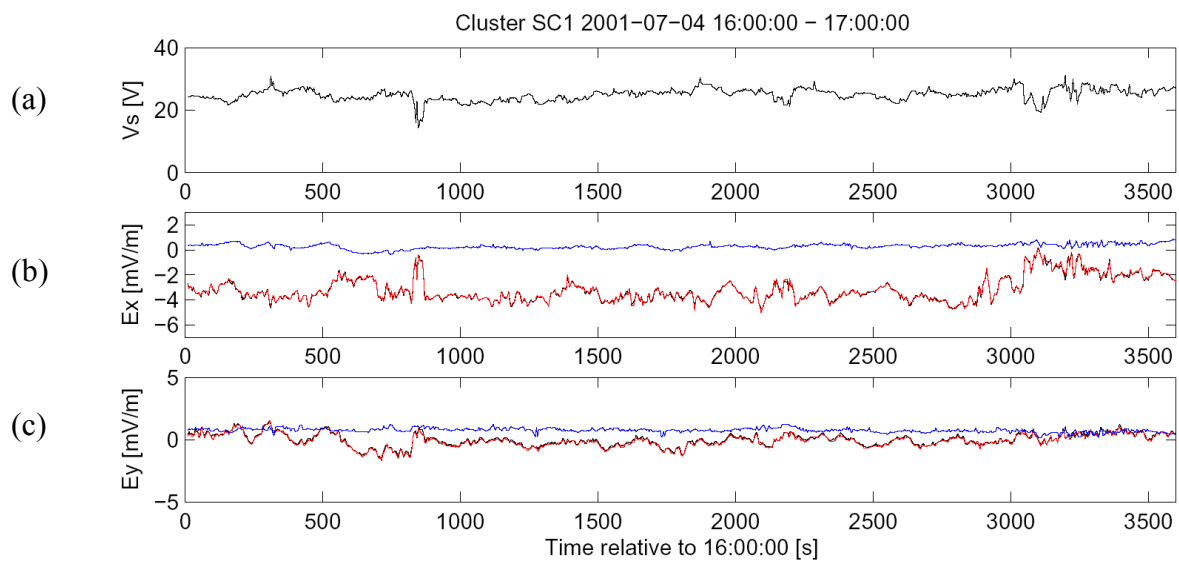

Figure 1. **Example plot of an interval where measurements of the electric field from the EFW (double-probe) and EDI (electron drift) instruments on Cluster differ. (a) Spacecraft potential V_s. (b) Electric field in the GSE X (sunward) direction from EFW (red and black) and EDI (blue). (c) Electric field in the GSE Y (duskward) direction in the same format.**

An example is shown in Figure 1. The data are from a position (1.6, -3.2, 7.9) R_E in GSE coordinates, which means Cluster is in the polar cap at a geocentric distance of 8.6 R_E, on magnetic field lines reaching into the northern geomagnetic tail lobe as illustrated in Figure 2. Panel (a) of Figure 1 shows the spacecraft potential V_s, estimated from the average voltage V_{ps} between the four EFW spherical probes and the spacecraft. As the application of a bias current ensures that the probes stays within one or two volts from the local plasma, the spacecraft potential $V_s \approx -V_{ps}$, where V_{ps} is the difference in potential between probes and spacecraft. The spacecraft potential depends strongly on the plasma density (Pedersen, 1995). For Cluster, the spacecraft potentials of 20 V to 30 V indicated here translates to approximate plasma densities between 1 cm^{-3} and 0.2 cm^{-3} (Pedersen et al., 2001). However, ion data from the Cluster Ion Spectrometer (CIS) (Rème et al., 2001) indicate much lower densities, well below 0.1 cm^{-3} throughout this interval (Eriksson et al., 2003). This can be explained by the presence of a cold plasma, with ion energies below eV_s, so that the ions cannot reach the

spacecraft. Such a plasma is indeed expected in this part of the magnetosphere, as this is the region of the cold plasma outflow known as the polar wind, studied by numerous spacecraft below a few Earth radii. Observations at higher altitudes are rare, as the low densities here give rise to high spacecraft potentials complicating direct observation of ions. However, by using artificial potential control of the POLAR satellite, Su et al. (1998) were able to study its properties at 8 R_E. Typical parameters for the proton component were found to be 0.3 cm^{-3} density, 45 km/s flow speed, and temperature 1 - 2 eV, resulting in a mean Mach number of 4.55. Oxygen and helium densities were lower by factors of around 6 and 38, respectively.

Panels (b) and (c) of Figure 1 show the GSE X and Y components of the electric field as derived from the EDI drift observations (blue) and from the EFW probe-to-probe voltages. The EFW data are plotted as two curves (black and red), derived by fitting a sinusoid to the signals observed in the rotating (4 second period) spacecraft frame by the two pairs of probes in the spin plane, P12 (black) and P34 (red). As the spacecraft spin axis is a few degrees from the GSE Z axis, the X and Y components actually are a few degrees off the corresponding GSE coordinate axes. The difference between EFW and EDI data in this time interval is apparent, reaching up to 5 mV/m. Comparisons to ion flow measurements show that in this case, the EDI data provide a good measurement of the natural electric field in the plasma, while EFW data are contaminated by potentials induced by the presence of the spacecraft (Eriksson et al., 2003). We may note that the source of this field is very stable in the sense that both EFW probe pairs provide essentially identical field estimates, as evidenced by the black and red lines in panels (b) and (c) lying on top of each other. It can be seen that in this case, the additional electric field points mainly in the -X direction, with a component in -Y. From the left panel in Figure 2, it is clear that a polar wind outflow along the magnetic field should be essentially in this direction in the spin plane, which is almost identical to the GSE XY plane. The direction is thus consistent with a wake-generated field.
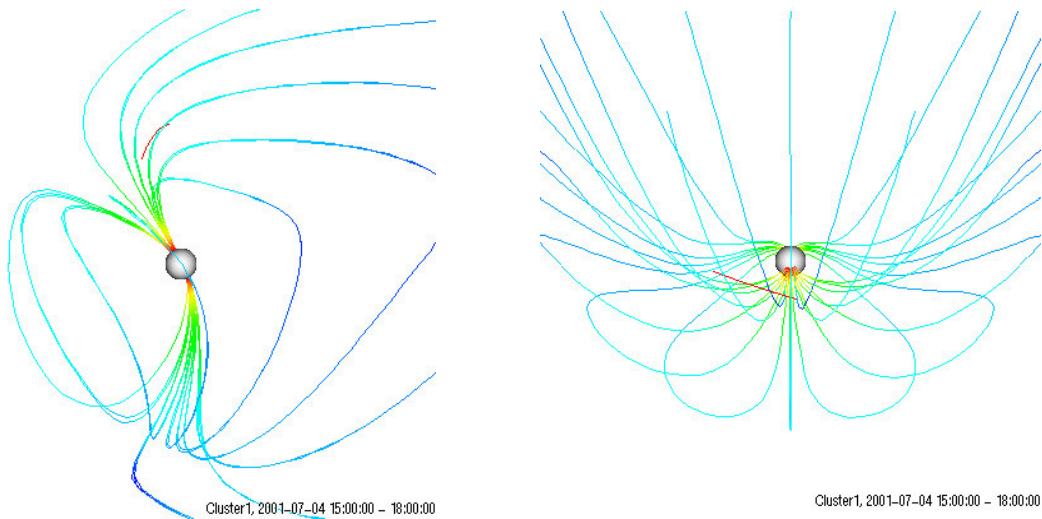

Figure 2. The red line marks the position of Cluster in the magnetosphere in the time interval 15:00 - 18:00 on July 4, 2001, as viewed from the GSE Y (left) and Z (right) directions. Some geomagnetic field lines are shown, colour coded for magnetic field intensity. Image produced using the orbit visualization tool, OVT (http://ovt.irfu.se), using IGRF and Tsyganenko-87 models for the magnetic field.

Perturbation potentials of this kind are commonly found to contaminate EFW data in the polar wind region and can sometimes be found also in other magnetospheric regions with a

cold tenuous plasma, but are rare in denser regions like the solar wind. In the solar wind, a wake may indeed form behind the spacecraft, but it is small and shows up as a pulse-like distortion of the EFW data when the probe passes through the wake. Such a wake poses no problem, while data like those shown in Figure 1 are not easily cleaned. Why is the wake problem so different in the two regions? The explanation lies in the relation between ion flow energy, $m_i v^2/2$, ion thermal energy KT_i, and spacecraft potential, V_s. In the solar wind, we certainly have $m_i v^2/2 > KT_i$ so that a wake is formed, but the plasma is sufficiently dense to ensure a low spacecraft potential, i.e. $eV_s < m_i v^2/2$. The ions can reach the spacecraft, and the transverse size of the wake is determined by the spacecraft geometry. In particular, the wire booms of 2.2 mm diameter cause a negligible wake. Now consider the case

$$eV_s > m_i v^2/2 > KT_i \qquad (1)$$

which is appropriate for the tenuous plasmas encountered by Cluster in the polar wind. The flow is supersonic and so a wake will form, but the size of this wake will now not be determined directly by the spacecraft mechanical structure but by the electrostatic equipotential $\Phi \approx m_i v^2/(2e)$ which no ions can climb. If we assume vacuum conditions, a spherical spacecraft of radius r at 20 V in a plasma with flow energy 5 V increases its effective size transverse to the ion flow from πr^2 to $16\,\pi r^2$, because the 5 V equipotential is at a distance of $4\,r$ from the centre of the spacecraft. This 16-fold increase in obstacle area may seem dramatic, but even more so is the effect on the wire booms. Assuming they behave like infinite cylinders of radius a in vacuum except for the potential going to exactly zero at a distance of $g\lambda_D$, where $g > 1$ is some real number, the potential field at radial distance r from a wire boom at potential V is

$$\Phi(r) = V\,\frac{\ln(r) - \ln(g\lambda_D)}{\ln(a) - \ln(g\lambda_D)} \qquad (2)$$

From this, we get the radial distance r_b at which $\Phi(r_b) = bV$, where $0 < b < 1$, as

$$r_b = a^b (g\lambda_D)^{(1-b)}. \qquad (3)$$

For the Cluster wire booms with $a = 1.1$ mm, a Debye length of 15 m, and an arbitrary but reasonable choice of $g = 2$, we get $r = 2.3$ m for the 5 V equipotential around a wire boom at 20 V. The effective size of the booms transverse to the flow therefore increases from 2.2 mm to 4.6 m, i.e. by three orders of magnitude. This increase depends to some extent on the arbitrary choice of g, but the effect is certainly significant for all realistic g. It is therefore possible that the normally neglegible wire booms supporting the EFW probes can become significant obstacles to the plasma flow in the conditions (1), as illustrated in Figure 3.

How large effects could such a wake have on double-probe electric field measurments? Considering a wake of slab-like geometry with thickness $d \ll \lambda_D$, we may assume perfect exclusion of ions and no impact on the electrons. Solving Poisson's equation gives a maximum potential in such a wake $\Phi_{\text{wake}} = (d/\lambda_D)^2\, KT_e/e$. For a wake of size $d \sim \lambda_D$ or larger, the potential saturates at $\Phi_{\text{wake}} \sim KT_e/e$, as further accumulation of electrons is inhibited. The
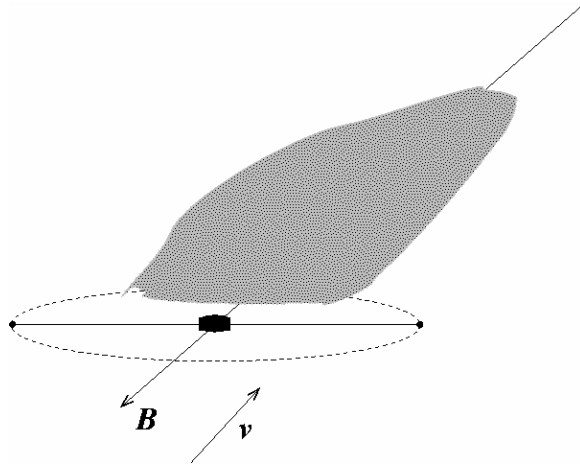
Figure 3. Sketch of a large scale wake forming behind the potential structure around a spacecraft equipped with wire booms at the same potential as the spacecraft, in the case of a plasma $eV_s > mv^2/2 > KT_i$ flowing along the magnetic field. The dashed line indicates the equipotential equivalent to the ion flow energy.

small wake with d on the order of millimeters found behind the booms in for example the solar wind thus cannot give rise to appreciable potentials, while it should be possible to get significant wake charging in the polar wind case of $eV_s > m_i v^2/2 > KT_i$. This wake field may impact on the measurements by a double-probe instrument in the way we have seen in the data presented above. An upper bound on the magnitude of this effect on the double-probe measurments can be obtained by assuming that one probe experiences the full wake potential while the other sees nothing, which would give a wake-induced electric field signal in the double-probe instrument of up to $KT_e/(2\ l\ e)$, where $2\ l$ is the separation between the two probes, i.e. 88 m for Cluster EFW. Assuming polar wind KT_e values of the order of a few tenths of eV, we find that wake-induced fields up to a few tens of mV/m could indeed be possible, which would explain the observations. However, to provide some more stable foundations to these estimates, we must go to simulations. This is the topic of Section 3 below.

We get evidence for the enhanced enhanced wake mechanism outlined above by studying intervals when the artificial potential control instrument ASPOC (Torkar et al., 2001) is operating. By emitting a current typically around 10 µA of keV ions, ASPOC stabilizes the spacecraft potential at around 8 V. Figure 4 shows data from two of the Cluster satelites, Cluster 1 (Rumba) in the top two panels and Cluster 3 (Samba) in the lower two. At the time shown, Cluster was above the northern polar cap at (-2.5, 1.4, 4.9) R_E in GSE coordinates. The environment is similar to that of Figure 1, though the peak V_s values of 40 V indicate densities down to 0.1 cm^{-3}. ASPOC is not operational on Cluster 1, but on Cluster 3, ASPOC is turned on close to 3250 s into the plot, resulting in an immediate and clearly visible stabilization of V_s. In the Cluster 1 data, EFW and EDI are seen to differ by up to 10 mV/m from 3000 s onwards. Only E_X is shown, as almost all the wake induced field turns up in this component because the magnetic field Y component is very small. The same EDI-EFW discrepancy initially occurs also on Cluster 3, but at the ASPOC turnon, the difference essentially vanishes. This is exactly the behaviour we should expect from a wake created by the spacecraft potential distribution as discussed above: when V_s decreases, so does the size of the wake and hence the perturbation it causes to the potential field around the spacecraft. The clear relation between the natural variations in spacecraft potential and the wake-induced field that can be seen in the Cluster 1 data shows that it really is V_s which is the controlling parameter, regardless of whether it is regulated by the plasma environment or by ASPOC.
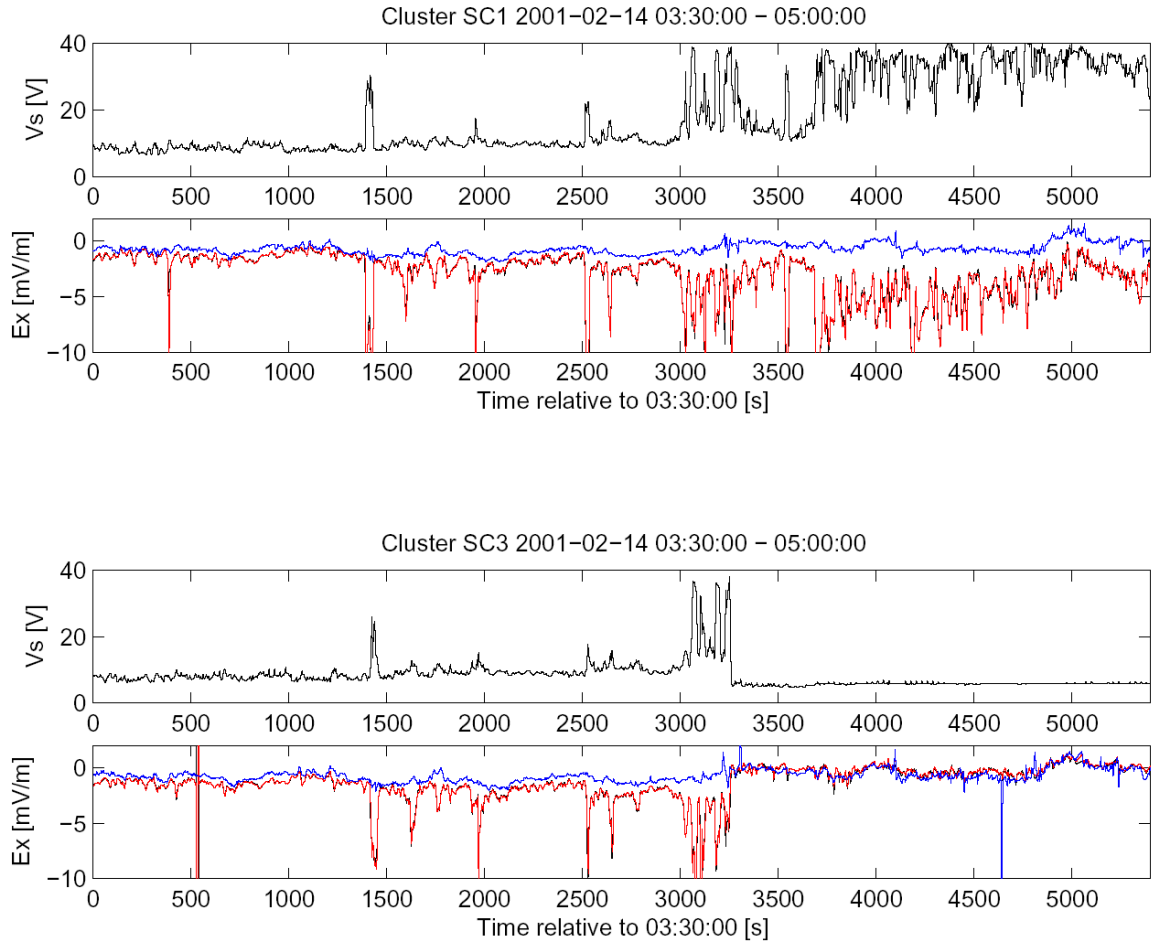
Figure 4. EFW and EDI electric field data from Cluster 1 (top two panels) and Cluster 3 (lower two). For each s/c, the top panel shows the spacecraft potential V_s, while the lower panel displays the EDI (blue) and EFW (red, black) estimates of the GSE X component of the electric field. The jump in V_s for Cluster 3 at 3250 s into the plot is due to ASPOC turning on. Strong discrepancies between the EDI and EFW electric field estimates can be seen from around 04:20. For Cluster 1, they continue throughout the interval, while they almost disappear in Cluster 3 data when ASPOC is turned on.

Simulations

We have used the simulation code package PicUp3D (Forest et al., 2001) to model the Cluster phenomena. This is a particle-in-cell code using a fixed homogeneous grid, assuming Dirichlet boundary conditions for the potential. PicUp3D does not self-consistently determine the potential of the spacecraft, but this is of no concern to us here as the density-potential relation is known (Pedersen et al., 2001). We have used common PCs (2.6 GHz AMD) with at most 0.5 GB of RAM allocated to the simulation. On these machines, the presented runs have typically taken around four days to complete.

In the simulation presented here the spacecraft is modelled as a single boom, neglecting the effects of the spacecraft body (Figure 5), in accordance with the discussion in Section 2 which suggested that the booms themselves may become significant obstacles to a cold flowing plasma. For this simulation we use the following plasma parameters:

- Plasma density, $n_0 = 0.15$ cm^{-3}
- Electron temperature, $KT_e = 1.8$ eV
- Ion temperature, $KT_i = 1.8$ eV
- Ion drift kinetic energy, $m_i v^2/2 = 9$ eV

These properties are consistent with the POLAR results (Su et al., 1998) cited above as well as with the Cluster observations in Figures 1 and 4. The Debye length becomes $\lambda_D \approx 26$ m and the electron plasma frequency $\omega_{pe}/(2\pi) \approx 4$ kHz. The ion drift kinetic energy corresponds to a flow velocity of $u = v_{th}^i \sqrt{10}$, which is taken to be in the y-direction. The magnetic field is neglected in the simulations, as the ion gyroradii are 1 km for protons and 5 km for O$^+$, both significantly larger than the scale of the problem and the simulation boxes. The electron gyroradius (30 m) is closer to the scale of the problem but has also been neglected, which possibly may cause some overestimation of the electron densities in the wake. We model only one ion species, with a mass ratio $m_i/m_e = 100$.

In general for these types of simulations, the size of the computational box is chosen as a compromise between the theoretical requirement that the boundary conditions for the potential should not affect the overall potential structure, and the practical desire to complete a normal simulation in less than a week. The boundary conditions are of Dirichlet type ($\Phi_b = 0$), which means that the walls of the computational box have to be sufficiently far away from the spacecraft. At a distance of $2\lambda_D$ the Debye shielding is supposed to have decreased the potential to a satisfactorily low level, why this is chosen to be the smallest distance from the spacecraft to any of the walls. Since the wake will be behind the spacecraft, the distance from the spacecraft to the far wall has to be much larger than this smallest distance. We will return to these limitations and their effect on the simulations below.
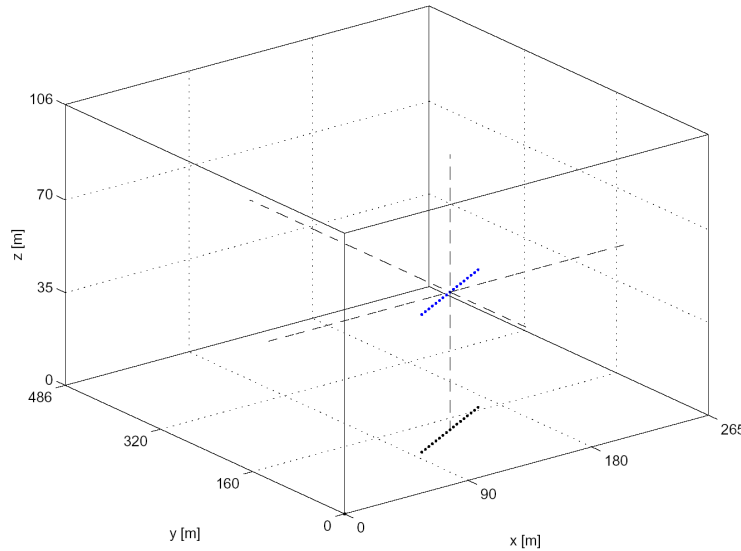

Figure 5. The boom in the computational box, which with the grid resolution of 4.4 m has the dimensions $x = 265$ m, $y = 486$ m, $z = 106$ m. The length of the boom is 100 m and is constituted of 17 discrete grid points (blue). The black dotted line is the projection of the boom on to the plane $z=0$.

For this specific run, the grid-size is approximately 4.4 x 4.4 x 4.4 m^3 and the number of grid-steps in each direction is $N_x=60$, $N_y=110$, $N_z=24$ (Figure 5). Thus, the dimensions of the computational box is $x = 265$ m, $y = 486$ m, $z = 106$ m, which all may be compared to $\lambda_D = 26$

m. To achieve a satisfactory accuracy in the simulations, the number of particles is adjusted so that there are in average 8 particles per box. The integration time step for the motion of the particles is set to $0.034/\omega_{pe}$. It is chosen in such a way that no particle cross a cell in less than a few time steps.

The boom is placed in the *xy*-plane with $z = 53$ m at an angle of 45° relative to the positive *x*-axis, which means that it has the same angle to the flow. This angle has been chosen as typical. As PicUp3D includes no explicit provisions for modelling booms, we have instead fixed the potential of 17 discrete grid points, extending from (x=97, y=97) to (x=168, y=168). This means that the boom in the simulations obtains a length of 100 m, close to the actual length 88 m. Each grid point on the boom is set to the potential +36 V, which is consistent with the situations in Figures 1 and 4, and with a plasma density of approximately 0.15 cm^{-3} (Pedersen et al., 2001). However, due to the grid resolution of 4.4 m, the decrease of the potential close to the boom is slower than expected from a real wire boom of 2.2 mm diameter, and we will show later in this paper that the choice of 36 V for the grid points modelling the boom actually may correspond to a thin wire boom as high as 50 V. Further simulations are needed to take this under estimation of the potential into account.

Results from the boom simulations are shown in Figures 6 and 7. The output data is averaged over the time period from $30/\omega_{pe}$ to the end of the simulation at $60/\omega_{pe}$ in order to obtain smoother plots. Figures 6 a-c show the potential around the boom in the planes z=53, x=133 and y=243 respectively. As can be seen most clearly in Figure 6a, the dominating structure is the decaying potential around the boom, giving essentially elliptic equipotentials down to 1 V. As expected, a negatively charged wake forms behind the boom, reaching a minimum potential of -0.69 V. The ion density in Figure 7a shows the same wake structure, while the effect most apparent in the density of electrons in Figure 7b is their agglomeration around the positive boom. A small depletion in the region of the wake can also be seen, as is expected for a wake approaching Debye length scale. It should be noted that the ions, whose energy is around 9 eV, do not care about the details of a wake potential at a few tenths of volts. This means that the ion density in Figure 7a results essentially from the potential from the booms, so that the ion density is only marginally affected by any possible influence from the Dirichlet boundary conditions on the potential. With a Mach number of √10, few ions can leak into the central wake from the boundaries aligned with the flow, so the effect of this boundary should also be small. However, it is clear that the Dirichlet conditions on the potential do to some extent influence the potential and the electron density, as the ion wake seen in Figure 7a extends out through the boundary. A run with half the simulation box size in the *z*-direction resulted in a potential minimum of only -0.24 V, verifying that we are at least close to the limit where the boundary conditions influence the result. Further simulations with larger grid will be needed to resolve this issue. We thus consider the -0.69 V wake potential observed in this simulation to be a lower bound rather than a true estimate. The influence of the far wake boundary conditions on the wake does not seem to be significant. This has been verified by a simulation with a much more elongated computational box in the flow direction (900 m). The dimensions in the other directions and the simulation parameters remained the same, but the grid size was increased to 8.8 m in each direction to obtain reasonable convergence times.
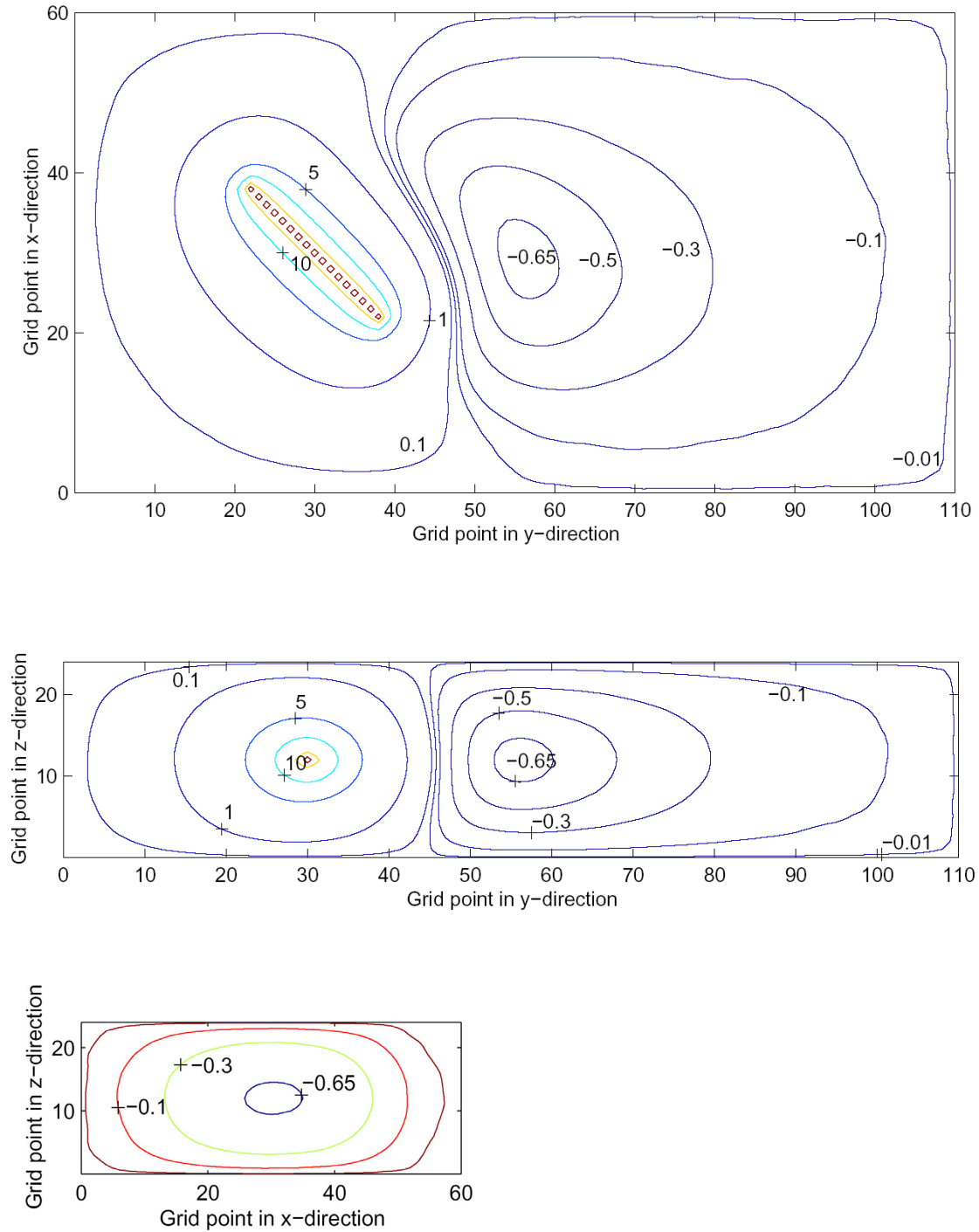
Figure 6. Contour plots of the potential for the boom simulations. The minimum value of the potential in the wake is -0.69 V. (a) Potential in the xy-plane with *z*=53. (b) Potential in the yz-plane with *x*=133. (c) Potential in the xz-plane with *y*=243. The grid spacing is 4.4 m.
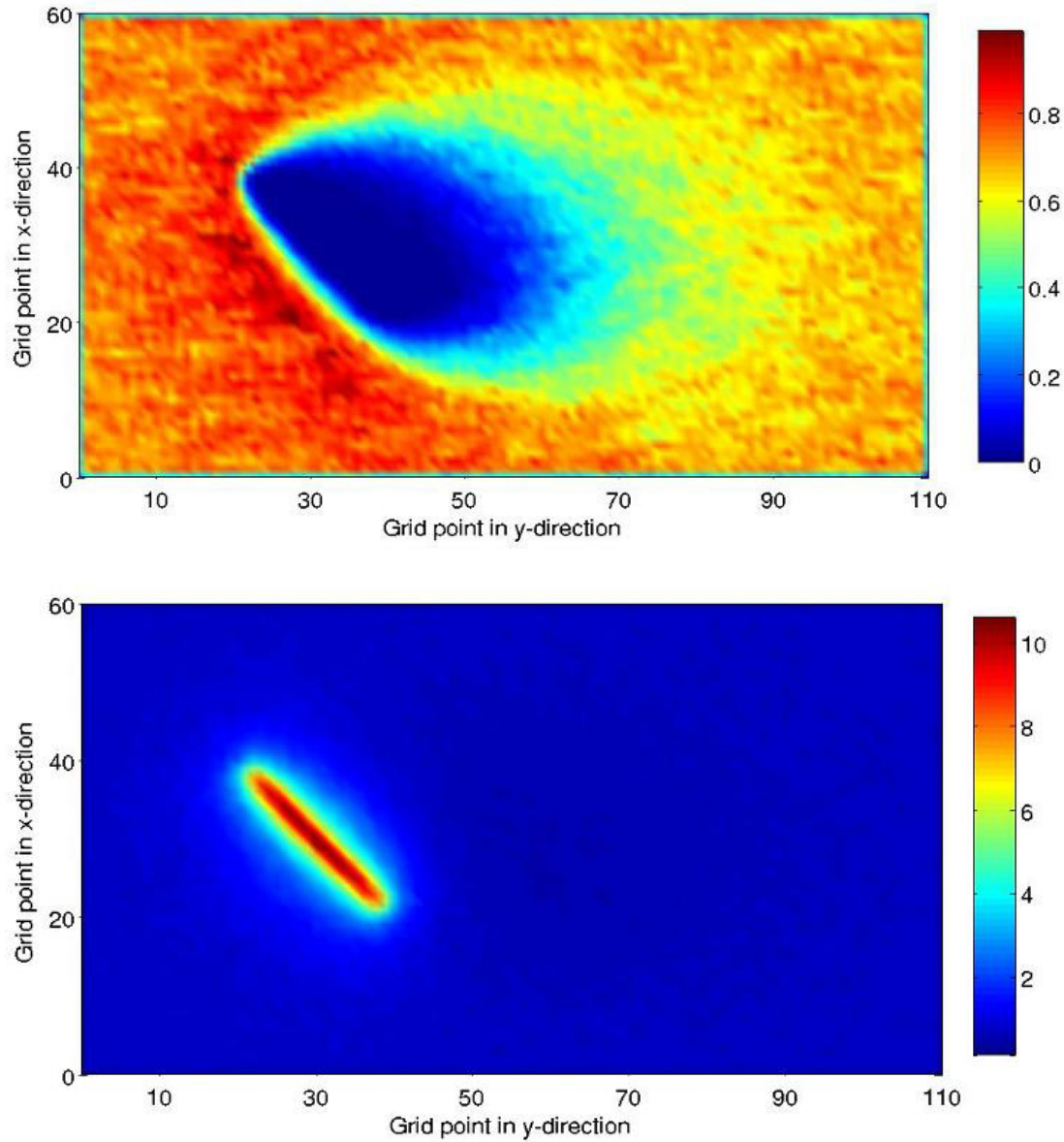
Figure 7. Densities of ions and electrons from the boom simulations. (a) Density of ions. (b) Density of electrons. The grid spacing is 4.4 m.

We will now use the simulation result to quantify the impact of the wake field on a double-probe electric field instrument. Such an instrument has one probe at each end of the boom, with bootstrapped elements in between to shield away the direct influence of the boom potential (Gustafsson et al., 2001). For Cluster EFW, the probes are 3 m outside the part of the wire booms which are at spacecraft potential. In Figure 8, we plot the difference in potential between two probes which are at the same distance from the opposite ends of the wire boom, as a function of this distance. The maximum potential difference is approximately 630 mV. One grid spacing distance (4.4 m) out from the boom on each side, which is close to the 3 m relevant for Cluster EFW, the observed potential difference between the probes is 490 mV. Dividing this by 100 m, we find that EFW could be expected to suggest an apparent electric field of 5 mV/m because of the wake. This is for the simulated boom angle with respect to the flow of 45°, but as the amplitude of the perturbation should vary with this angle, reaching a maximum at 0° and 180°, the wake induced field in spin fitted data like in Figures 1 and 4 could be expected to be somewhat larger, around 6 or 7 mV/m. This is close to the observed EFW-EDI discrepancies in Figure 1, though we should remember that the

plot in Figure 8 is based on a simulation with 4.4 m grid resolution. This cannot possibly catch all detail a few meters from the ends of the wire booms, but in as far as the difference results from the large scale properties of the wake, not from the details close to the probe positions, we may expect the result to be correct at least as an order of magnitude estimate.

(a)   (b)
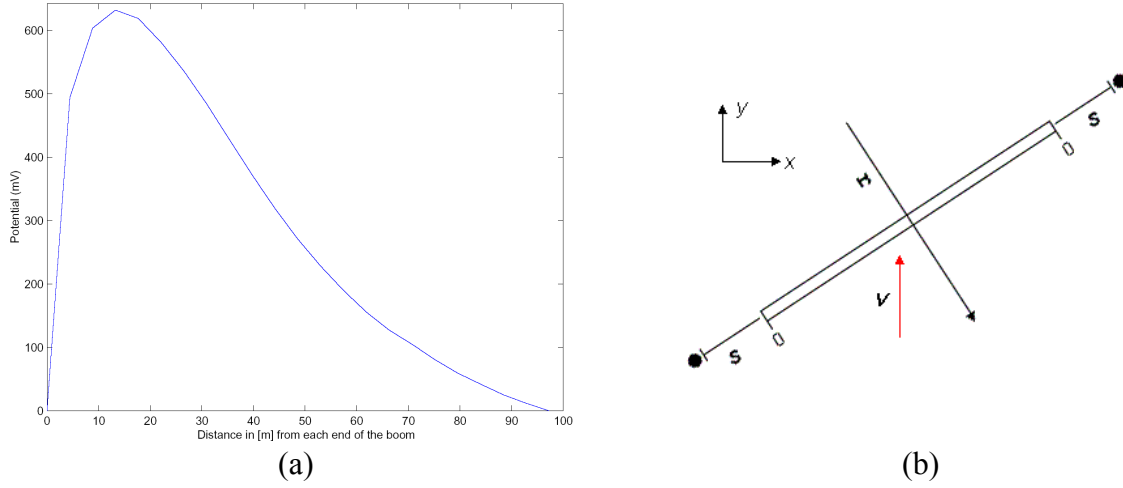
Figure 8. (a) Difference in potential between the ends of the boom. The maximum potential difference is 630 mV. (b) Schematic picture of the boom explaining the horizontal axis of (a): *s* is the distance from the boom end to the probe. The coordinate *r* is the radial distance from the midpoint of the boom used in Figure 9.

As have been mentioned above, the grid spacing of 4.4 m will result in the potential close to the boom attaining larger values than would have been the case for a real wire boom (2.2 mm diameter for Cluster EFW) at 36 V. At a distance of several Debye lengths from the boom, we may expect the simulation result to be the true potential, but not close to the boom. To compensate for this discrepancy, an effective boom potential is calculated by comparison with analytical models. At high potentials close to the boom the Debye shielding has only small effects and the boom potential can be compared with the vacuum potential of a thin cylinder. According to Hallén (1929), the vacuum potential of a thin cylinder at potential V is

$$\Phi(x', y', z') = \frac{V}{2\ln\left(\dfrac{l}{a}\right)} \ln\left(\frac{d - x' + r_1}{-d - x' + r_2}\right), \qquad (4)$$

where l is the length of the cylinder which is aligned with the x axis and centred on the origin, a is its radius, $d = l/2$, $r_1 = [(x'-d)^2 + y'^2 + z'^2]^{1/2}$ and $r_2 = [(x'+d)^2 + y'^2 + z'^2]^{1/2}$. We now look for a value of V in this expression that result in a potential approximately like the simulation result around 9 V and a few volts below, as this should be the most sensitive region for the dynamics of the ions, whose drift energy is 9 eV. Figure 9 shows a plot of the simulated potential (dashed blue) together with the analytic model for a thin boom potential of 52 V (black), with radial distance from the midpoint of the boom on the horizontal axis. It can be seen that this indeed approximates the simulated potential field around and below 9 V, and it may therefore be that the potential of 36 V applied to the point cluster simulating the booms corresponds to an actual potential as high as 50 V for a real wire boom.

Further away from the boom, (4) does not give a correct picture, because of the Debye shielding in the plasma. Therefore it is adequate to also compare the simulated boom potential to that of a Debye shielded infinite cylinder, which takes the form

$$\Phi(r) = V \frac{K_0\left(\dfrac{r}{\lambda_D}\right)}{K_0\left(\dfrac{a}{\lambda_D}\right)},\tag{5}$$

where r is the perpendicular distance from the boom, a is the radius of the boom and K_0 a modified Bessel function of the second kind. Figure 9 shows the potential as a function of the perpendicular distance from the middle of the boom for the simulated boom potential, the Hallén potential and the Debye shielded potential. As expected, the Hallén model and the shielded cylinder approach each other far from the boom. Closer to the boom, the Debye shielding expression (5) breaks down because of violation of the assumption $e\Phi << KT_e$ inherent in the linear Debye shielding law. The influence of the wake on the potential can clearly be seen in the asymmetry of the simulation data.
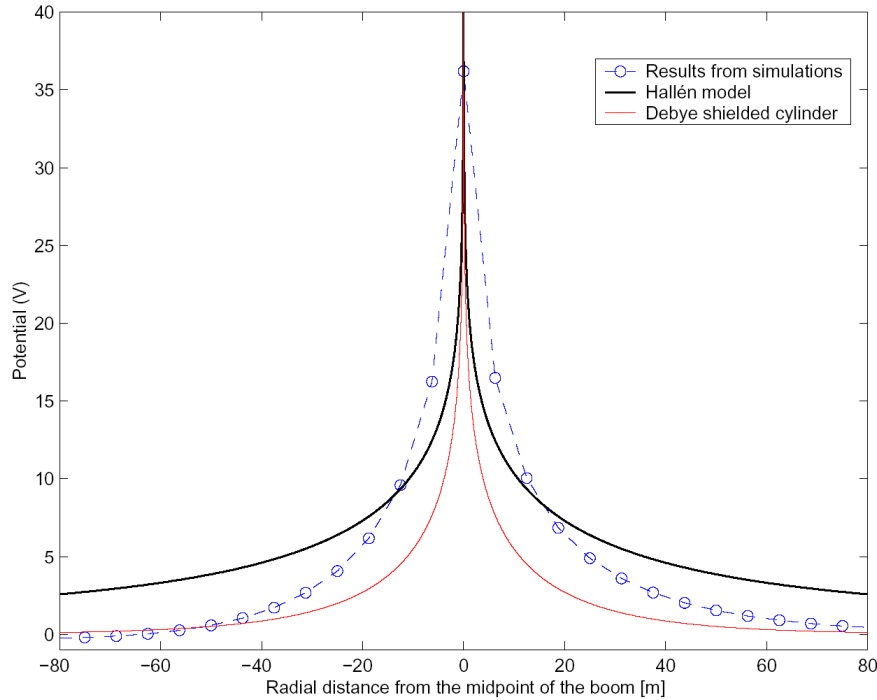

Figure 9. Comparison between the potential obtained from the simulation (dashed blue) and analytical models. The red line corresponds to an infinite Debye shielded cylinder and the black line to the model introduced by Hallén. The horizontal axis gives the radial distance from the center of the boom in the boom-flow plane (r in Figure 8b).

Discussion and Conclusion

In this paper, we have presented experimental data from the EFW and EDI electric field instruments on Cluster, showing some examples where EFW observes an electric field which to a large extent, or even dominantly, is not of geophysical origin. As such phenomena are not uncommon in the EFW data set in some regions of the magnetosphere, they are important

to understand to ensure maximal scientific return from the instrument. A model where the additional electric field seen by EFW is explained in terms of an electrostatic wake of enhanced size forming behind the wire booms when $eV_s > m_i v^2/2 > KT_i$ was introduced and found to be consistent with a number of features in the data, including the direction of the non-geophysical field, its dependence on spacecraft potential including its decay when this potential is controlled by the ASPOC instrument, and its presence in a region known to contain the cold and tenuous supersonic plasma flow of the polar wind. More detailed investigations of the experimental data is provided by Eriksson et al. (2003). We derived some analytical estimates of the magnitude of the effect at the end of Section 2, and went on to numerical simulations in Section 3. The simulations indeed verified the qualitative hypothesis, showing the generation of a negatively charged wake behind the spacecraft.

An attempt to derive the non-geophysical field observed by EFW resulted in 5-7 mV/m, which is close to observed magnitudes. Future work should include the effect of biasing and bootstrapping of the mechanical elements between the probe and the boom tip, which may have some impact on this value. However, for detailed studies of the influence of the near-probe environment, a more flexible grid is necessary. Potentially important factors not included in the present simulation also include the emission and exchange of photoelectrons by different electrical elements on the spacecraft. It is for example possible that the wake to a large extent is filled by photoelectrons emitted from the probes rather than by natural plasma electrons.

The simulations presented here leave several issues to be settled, and further work is necessary. Nevertheless, we have been able to verify the qualitative idea of an enhanced electrostatic wake, and got reliable results at least for the ion densities around the spacecraft. Our main conclusions from this work can be stated as follows:

1. The qualitative hypothesis of an electrostatic wake with dimensions determined by the spacecraft potential field forming in situations with $eV_s > m_i v^2/2 > KT_i$ is consistent with data.

2. Numerical simulations verify the qualitative picture, and have produced lower bounds on the induced wake potentials.

3. We consider the results from the simulations reliable in the entire simulation region for the ion density, but not for the potential, mainly because of influence from the boundary conditions. However, our main interest is the region close to the spacecraft, where impact of the boundaries should be smaller. Further simulations with varying grid size are needed to verify this. The main limitation of the used grid is its extension out of the plane containing the booms and the flow, which is the principal direction in which the ions are deflected by a quasi-cylindrical potential distribution around the boom.

4. The PicUp3D code proved very handy for this type of study. It is unlikely that we would have undertaken this venture without a code we can run on our workstations, and the open source is a major advantage for scientific use.

5. For this kind of problem, we consider the main technical limitation of PicUp3D to be that it only handles Dirichlet conditions on the potential. For a wake extending far from the spacecraft, Neumann conditions on all sides except the inflowing boundaries would be more suitable.

6. The inability of a fixed grid code to model thin booms leads to an under estimation of the simulated boom potential. This issue can in future simulations to some extent be circumvented by introducing an effective potential, using comparison to analytical expressions. The validity of the method using effective potentials should be verified by comparison to adaptive-grid codes.

7. From the simulation results, we have extracted an estimate of the wake-induced electric field signal observed from a pair of probes outside the ends of the modelled booms, assuming the probes perfectly couple to the plasma.

Acknowledgements

References

1. Eriksson, A., M. André, B. Klecker, H. Laakso, P.-A. Lindqvist, F. Mozer, G. Paschmann, A. Pedersen, J. Quinn, R. Torbert, K. Torkar, and H. Vaith, Cluster comparison of the double-probe and electron drift techniques for measuring the electric field, manuscript in preparation, 2003.

2. Escoubet, C. P., M. Fehringer, and M. Goldstein, The Cluster mission. *Annales Geophysicae, 19,* 1197 - 1200, 2001.

3. Forest, J., Eliasson, L., and Hilgers., A., A New Spacecraft Plasma Simulation Software, PicUp3D/Spis, in *Proceedings of the 7th Spacecraft Charging and Technology Conference,* ESA/SP-476, 515-520, 2001.

4. Gustafsson, G., et al., The Electric Field and Wave Experiment for the Cluster Mission. *Space Science Reviews, 79,* 137 - 156, 1997.

5. Gustafsson, G., et al., First results of electric field and density observations by Cluster EFW based on initial months of operation. *Annales Geophysicae, 19,* 1219 - 1240, 2001.

6. Hallén, E., Lösung zweier Potentialprobleme der Elektrostatik*, Arkiv för matematik, astronomi och fysik, 21A*, 22, 1929.

7. Paschmann, G., C. E. McIlwain, J. M. Quinn, R. B. Torbert, and E. C. Whipple, The Electron Drift Technique for Measuring Electric and Magnetic Fields. *Measurement Techniques in Space Plasmas: Fields*, AGU Geophysical Monograph 103, 1998.

8. Paschmann, G., et al., The Electron Drift Instrument on Cluster: overview of first results. *Annales Geophysicae, 19,* 1273 - 1288, 2001.

9. Pedersen, A.: Solar wind and magnetosphere plasma diagnostics by spacecraft electrostatic potential measurements, *Annales Geophysicae*, 13, 118–121, 1995.

10. Pedersen, A., F. Mozer, and G. Gustafsson: Electric Field Measurements in a Tenuous Plasma with Spherical Double Probes. *Measurement Techniques in Space Plasmas: Fields*, AGU Geophysical Monograph 103, 1-12, 1998.

11. Pedersen, A., et al., Four-point high time resolution information on electron densities by the electric field experiments (EFW) on Cluster, *Annales Geophysicae,* 19, 1483-1489, 2001.

12. Rème, H., et al., First multispacecraft ion measurements in and near the Earth's magnetosphere with the identical Cluster ion spectrometry (CIS) experiment, *Annales Geophysicae, 19,* 1303, 2001

13. Su, Y.-J.; Horwitz, J.L.; Moore, T.E.; Giles, B.L.; Chandler, M.O.; Craven, P.D.; Hirahara, M.; Pollock, C.J., Polar wind survey with the Thermal Ion Dynamics Experiment/Plasma Source Instrument suite aboard POLAR, *Journal of Geophysical Research, 103*, 29305-29337, 1998.

14. Torkar, K., et al., Active spacecraft potential control for Cluster - implementation and first results, *Annales Geophysicae, 19,* 1289, 2001